Electrochemical Fenton-based treatment of tetracaine in synthetic and urban wastewater using active and non-active anodes

Carlota Ridruejo, Francesc Centellas, Pere L. Cabot, Ignasi Sirés**, Enric Brillas*

Laboratori d'Electroquímica dels Materials i del Medi Ambient, Departament de Química Física, Facultat de Química, Universitat de Barcelona, Martí i Franquès 1-11, 08028 Barcelona, Spain

Corresponding author: ** i.sires@ub.edu (I. Sirés)

* brillas@ub.edu (E. Brillas)

Abstract

The electrochemical degradation of tetracaine hydrochloride has been studied in urban wastewater. Treatments in simulated matrix with similar ionic composition as well as in 0.050 M Na_2SO_4 were comparatively performed. The cell contained an air-diffusion cathode for H_2O_2 electrogeneration and an anode selected among active Pt, IrO_2-based and RuO_2-based materials and non-active boron-doped diamond (BDD). Electrochemical oxidation with electrogenerated H_2O_2 (EO-H_2O_2), electro-Fenton (EF) and photoelectro-Fenton (PEF) were comparatively assessed at pH 3.0 and constant current density. The pharmaceutical and its byproducts were oxidized by $^{\bullet}OH$ formed from water oxidation at the anode surface and in the bulk from Fenton's reaction, which occurred upon addition of 0.50 mM Fe^{2+} in all media, along with active chlorine originated from the anodic oxidation of Cl^- contained in the simulated matrix and urban wastewater. The PEF process was the most powerful treatment regardless of the electrolyte composition, owing to the additional photolysis of intermediates by UVA radiation. The use of BDD led to greater mineralization compared to other anodes, being feasible the total removal of all organics from urban wastewater by PEF at long electrolysis time. Chlorinated products were largely recalcitrant when Pt, IrO_2-based or RuO_2-based anodes were used, whereas they were effectively destroyed by BDD($^{\bullet}OH$). Tetracaine decay always obeyed a pseudo-first-order kinetics, being slightly faster with the RuO_2-based anode in Cl^- media because of the higher amounts of active chlorine produced. Total nitrogen and concentrations of NH_4^+, NO_3^-, ClO_3^-, ClO_4^- and active chlorine were determined to clarify the behavior of the different electrodes in PEF. Eight intermediates were identified by GC-MS and fumaric and oxalic acids were quantified as final carboxylic acids by ion-exclusion HPLC, allowing the proposal of a plausible reaction sequence for tetracaine mineralization by PEF in Cl^--containing medium.

Keywords: BDD; Electro-Fenton; Photoelectro-Fenton; Product identification; Tetracaine; Urban wastewater

1. Introduction

The removal of pharmaceuticals and their metabolites from water bodies is an urgent challenge in order to improve the overall quality of drinking water. Pharmaceuticals enter continuously into the aquatic environment, pre-eminently from excreted feces and urine by either animals or humans, where they become accumulated at low contents around $\mu g\ L^{-1}$. This causes global alarm because of their possible long-term effects on living beings (Sirés and Brillas, 2012; Feng et al., 2013; Rivera-Utrilla et al., 2013; Golovko et al., 2014). Conventional biological and physicochemical systems that are ubiquitous in current wastewater treatment plants (WWTPs) result rather inefficient for destroying pharmaceuticals, thus remaining as micropollutants in natural water. This is the case of tetracaine ($C_{15}H_{24}N_2O_2$, 2-dimethylaminoethyl-4-butylaminobenzoate, M = 264.36 g mol^{-1}), an amino ester compound widely used for nerve block, as well as for spinal and topical anaesthesia. It is commercialized as hydrochloride salt and can be formulated as the base of ointments, gels and creams (Al-Otaibi et al., 2014; Shubha and Puttaswamy, 2014). The analysis of hospital wastewater has shown the presence of up to 0.48 $\mu g\ L^{-1}$ tetracaine (Escher et al., 2011). Powerful treatments are then needed for its removal from wastewater.

Electrochemical advanced oxidation processes (EAOPs) based on electrogenerated H_2O_2, with or without addition of catalytic Fe^{2+}, include electrochemical oxidation with electrogenerated H_2O_2 (EO-H_2O_2), electro-Fenton (EF) and photoelectro-Fenton (PEF), which have received increasing attention over the last years for treating wastewater containing organics (Brillas et al., 2009; Panizza and Cerisola, 2009; Oturan and Aaron, 2014; Sirés et al., 2014; Vasudevan and Oturan, 2014). These EAOPs are environmentally friendly because no noxious chemicals are employed and they originate powerful, short lifetime reactive oxygen species (ROS), mainly hydroxyl radical ($^{\bullet}OH$). This radical with E^{o} = 2.8 V/SHE can non-selectively attack most organics up to their overall mineralization (Martínez-Huitle et al., 2015; Moreira et al., 2017). The common feature of these methods is the continuous electrogeneration of H_2O_2 by reaction (1) from direct injection or

dissolution of O_2 gas that is reduced at a carbonaceous cathode such as boron-doped diamond (BDD) (Cruz-González et al., 2010, 2012), carbon-polytetrafluoroethylene (PTFE) O_2 or air-diffusion electrodes (Ammar et al., 2006; Thiam et al., 2014, 2015b), carbon felt (Dirany et al., 2012; El-Ghenymy et al., 2014; Yahya et al., 2014), carbon modified with metals or metal oxides nanoparticles (Assumpção,et al., 2013), graphite felt (Vatanpour et al., 2009), carbon nanotubes (Khataee et al., 2013, 2014) and activated carbon fiber (Wang et al., 2008).

$$O_2(g) + 2\,H^+ + 2e^- \rightarrow H_2O_2 \quad (1)$$

The studies performed in our laboratory with a carbon-PTFE air-diffusion cathode have shown its superiority over other electrodes for enhancing O_2 reduction, as well as for minimizing the cathodic reduction of organics. In EO-H_2O_2, EF and PEF performed in aqueous medium with sulfate anions, organics are preferentially oxidized by adsorbed hydroxyl radicals (M($^\bullet$OH)) formed at high applied current at the surface of a large O_2-overvoltage anode M from water oxidation (Boye et al., 2002; Marselli et al., 2003; Panizza and Cerisola, 2009):

$$M + H_2O \rightarrow M(^\bullet OH) + H^+ + e^- \quad (2)$$

Non-active BDD thin-film electrodes have been established as the best anodes for the production of physisorbed M($^\bullet$OH) from reaction (2) (Cañizares et al., 2005; Flox et al., 2006; Özcan et al., 2008). This is related to the very large overvoltage for O_2 evolution in aqueous medium and the weak $^\bullet$OH adsorption on its surface (Santos et al., 2010; dos Santos et al., 2015). This allows the generation of larger amounts of active M($^\bullet$OH) compared to other anodes, leading to greater mineralization of aromatics including pharmaceuticals (El-Ghenymy et al., 2013; Brinzila et al., 2014; Bedolla-Guzman et al., 2016; Coria et al., 2016). Conversely, active electrodes like Pt and dimensionally stable anodes (DSA®) based on IrO_2 and RuO_2 present lower oxidation ability because they yield less active, chemisorbed M($^\bullet$OH) that mainly appear as a weaker oxidant (i.e.,

superoxide species, MO) (Ribeiro et al., 2008; Panizza and Cerisola, 2009; Scialdone et al., 2009; Thiam et al., 2015a).

In chlorinated medium, Cl^- is oxidized to active chlorine species (Cl_2, HClO and/or ClO^-) from reactions (3)-(5), which compete with adsorbed M(•OH) to destroy the organic matter (Panizza and Cerisola, 2009; Martínez-Huitle et al., 2015). Under these conditions, DSA® anodes such as those based on RuO_2 form larger amounts of active chlorine to rapidly attack the aromatic molecules, even more quickly than BDD(•OH), although partial mineralization is achieved due to the accumulation of persistent chloroderivatives (Thiam at al., 2014; Steter et al., 2016).

$$2\ Cl^- \rightarrow Cl_2(aq) + 2e^- \quad (3)$$

$$Cl_2(aq) + H_2O \rightarrow HClO + Cl^- + H^+ \quad (4)$$

$$HClO \leftrightarrows ClO^- + H^+ \qquad pK_a = 7.56 \quad (5)$$

In EO-H_2O_2, M(•OH) and/or active chlorine are the main oxidizing agents, whereas the EF process becomes more powerful because it allows the generation of large amounts of •OH from Fenton's reaction (6), with optimum pH ~ 3, upon addition of a small quantity of Fe^{2+} as catalyst to the solution (Dirany et al., 2012; Yahya et al., 2014; Thiam et al., 2015b). •OH thus produced in the bulk is the most important oxidizing ROS in EF since it is continuously formed thanks to cathodic Fe^{2+} regeneration via reaction (7). The degradation can be upgraded if the solution is illuminated with UVA light in the PEF process. This irradiation causes the photolysis of $Fe(OH)^{2+}$, which is the preferential Fe^{3+} species at pH ~ 3, to be reduced to Fe^{2+} producing additional •OH by reaction (8). A more important role of UVA light is related to the photodecarboxylation of Fe(III) complexes with several carboxylic acids generated during the degradation process by the general reaction (9) (Moreira et al., 2013; Bedolla-Guzman et al., 2016; Coria et al., 2016).

$$H_2O_2 + Fe^{2+} \rightarrow Fe^{3+} + {}^{\bullet}OH + OH^- \quad (6)$$

105 $Fe^{3+} + e^- \rightarrow Fe^{2+}$ (7)

106 $Fe(OH)^{2+} + h\nu \rightarrow Fe^{2+} + {}^{\bullet}OH$ (8)

107 $Fe(OOCR)^{2+} + h\nu \rightarrow Fe^{2+} + CO_2 + R^{\bullet}$ (9)

108 The application of PEF to wastewater remediation has been pre-eminently focused on the
109 treatment of organic pollutants in synthetic solutions (Sirés and Brillas, 2012; Moreira et al., 2017),
110 whereas less is known about its oxidation power in real effluents like urban wastewater. The
111 complex composition of the latter matrices entails a greater difficulty for a clear interpretation of
112 the role of generated oxidants. Hence, comparison with simulated media is required to assess the
113 performance of PEF regarding pharmaceutical removal from real wastewater.

114 This paper presents a study on the degradation of tetracaine by means of EO-H_2O_2, EF and PEF
115 in acidic media. These treatments were comparatively performed in two kinds of synthetic
116 solutions: 0.050 M Na_2SO_4 to analyze the oxidation power of generated hydroxyl radicals and a
117 simulated matrix with chloride + sulfate ions to understand the action of active chlorine. These
118 trials were made to better understand the degradation of the pharmaceutical in an urban wastewater
119 matrix that contained main ions at a concentration similar to that of the simulated matrix, apart from
120 natural organic matter (NOM, related to tannic, fulvic and humic acids). The comparative oxidation
121 power of four anodes including BDD, Pt, IrO_2-based and RuO_2-based materials was tested using an
122 undivided cell with a carbon-PTFE air-diffusion cathode. The tetracaine decay and final carboxylic
123 acids were monitored by reversed-phase and ion-exclusion high-performance liquid
124 chromatography (HPLC), respectively. Primary intermediates formed in PEF with a BDD anode
125 using the simulated matrix were identified by gas chromatography-mass spectrometry (GC-MS),
126 allowing the proposal of a mineralization route for tetracaine. The evolution of total nitrogen and
127 ions concentrations during the PEF treatments in simulated matrix and urban wastewater as well as
128 the accumulated active chlorine content were determined as well.

2. Experimental

2.1. Reagents

Tetracaine hydrochloride ($C_{15}H_{24}N_2O_2 \cdot HCl$, M = 300.82 g mol^{-1}), heptahydrated iron(II) sulfate, dihydrated oxalic acid and fumaric acid were of analytical grade purchased from Sigma-Aldrich. The salts used as background electrolytes in the synthetic solutions were of analytical grade supplied by Probus, Prolabo and Panreac. These solutions were prepared with high-purity Millipore Milli-Q water with resistivity > 18 MΩ cm at 25 ºC. Analytical grade sulfuric acid from Merck was used to adjust the initial pH to 3.0. All the other chemicals were of analytical or HPLC grade supplied by Panreac and Merck.

2.2. Aqueous media

The following aqueous matrices were used in the electrolytic trials:

(i) A sample from the secondary effluent of a WWTP located in Gavà-Viladecans (Barcelona, Spain), which treasd 50,000 m^3 d^{-1} of urban and industrial wastewater. After collection and before use, it was preserved in a refrigerator (4 ºC). This real wastewater of pH = 8.1 and conductivity = 1.73 mS cm^{-1} had a total organic carbon (TOC) content = 12.2 mg L^{-1}. The concentration of cations was: 0.19 mg L^{-1} Fe^{2+}, 24 mg L^{-1} Mg^{2+}, 86 mg L^{-1} Ca^{2+}, 34 mg L^{-1} K^+, 212 mg L^{-1} Na^+ and 36.9 mg L^{-1} NH_4^+. The content of anions was: 0.79 mg L^{-1} NO_2^-, 0.85 mg L^{-1} NO_3^-, 318 mg L^{-1} Cl^- and 141.3 mg L^{-1} SO_4^{2-};

(ii) A simulated matrix that mimicked the real wastewater, prepared with Millipore Milli-Q water containing the following salts: 1.50 mM NH_4Cl, 10.0 mM NaCl, 0.50 mM K_2SO_4, 80.0 mM Na_2SO_4 and 0.02 mM $NaNO_3$. This solution of pH = 5.1 and conductivity = 1.79 mg L^{-1} did not contain any organic matter;

(iii) A 0.050 M Na_2SO_4 solution in Millipore Milli-Q water at pH = 7 with conductivity = 6.89 mS cm^{-1}, which was utilized for comparative purposes.

153 The pH of all the above solutions was adjusted to 3.0 before the electrolytic assays. Hence, the
154 conductivity of the three matrices increased up to 2.22, 2.01 and 7.53 mS cm^{-1}, respectively, values
155 that did not vary significantly during the electrochemical treatments.

156 *2.3. Electrochemical systems*

157 All the EO-H_2O_2, EF and PEF assays were carried out in a conventional undivided glass cell
158 surrounded with a jacket to keep the temperature at 35 ºC upon recirculation of thermostated water.
159 The cell contained 150 mL of solution, which was vigorously stirred with a magnetic bar at 800
160 rpm. Four anodes were alternately used: a boron-doped diamond (BDD) thin film over Si from
161 NeoCoat (Le-Chaux-de-Fonds, Switzerland), a Pt sheet (99.99% purity) from SEMPSA (Barcelona,
162 Spain), and IrO_2-based and RuO_2-based plates from NMT Electrodes (Pinetown, South Africa). The
163 cathode was a carbon-PTFE air-diffusion electrode from Sainergy Fuel Cell (Chennai, India) and
164 was fed with air at 1 L min^{-1} for continuous H_2O_2 generation, as previously reported (Thiam et al.,
165 2015a; Steter et al., 2016). The geometric area of all electrodes was 3 cm^2, whereas the
166 interelectrode gap was near 1 cm. The runs were made at constant current density (*j*), which was
167 supplied by an Amel 2049 potentiostat-galvanostat, being the cell voltage measured with a
168 Demestres 601BR digital multimeter. All the electrodes were initially cleaned/activated upon
169 polarization in 0.050 M Na_2SO_4 at j = 100 mA cm^{-2} for 180 min. The EF and PEF treatments of all
170 aqueous solutions were performed after addition of 0.50 mM Fe^{2+}, which is the optimum content of
171 this ion found for many organics degraded by these EAOPs in this kind of cell (Thiam et al., 2014,
172 2015a, 2015b)]. For PEF, the solution was exposed to UVA light (λ_{max} = 360 nm) provided by a
173 Philips TL/6W/08 fluorescent black light blue with a power density = 5 W m^{-2}, measured with a
174 Kipp&Zonen CUV 5 UV radiometer.

175 *2.4. Analytical methods*

176 A Metrohm 644 conductometer was employed to determine the electrical conductance of all
177 solutions, whereas their pH was measured with a Crison GLP 22 pH-meter. The H_2O_2 concentration

accumulated was determined from the light absorption of its Ti(IV) complex at λ = 408 nm using an Unicam UV/Vis spectrophotometer at 25 ºC (Welcher, 1975). All the samples were filtered with 0.45 μm PTFE membrane filters from Whatman before analysis. TOC of the samples was immediately measured on a Shimadzu VCSN TOC analyzer. Values with ±1% accuracy were found by injecting 50 μL aliquots into the analyzer. Total nitrogen (TN) was determined on a Shimadzu TNM-1 unit coupled to the TOC analyzer.

The tetracaine removal was monitored by reversed-phase HPLC. Acetonitrile (1:1) was added to the samples upon withdrawal during EF and PEF trials in order to stop the degradation process. This analysis was made by injecting 10 μL aliquots into a Waters 600 LC coupled to a Waters 996 photodiode array detector selected at λ = 311 nm. The LC was fitted with a BDS Hypersil C18 (250 mm × 4.6 mm) column at 25 ºC. The mobile phase was a 50:50 (v/v) acetonitrile:water (KH_2PO_4 10 mM, pH 3) mixture eluting at 1.0 mL min^{-1}. Under these conditions, the chromatograms exhibited a well-defined peak for tetracaine at retention time t_r = 8.9 min. The generated carboxylic acids were quantified by ion-exclusion HPLC using the above LC fitted with a Bio-Rad Aminex HPX 87H (300 mm × 7.8 mm) column at 35 ºC, setting the photodiode array detector at λ = 210 nm and eluting a 4 mM H_2SO_4 solution as mobile phase at 0.6 mL min^{-1}. Well-defined peaks related to fumaric (t_r = 14.7 min) and oxalic (t_r = 6.8 min) acids were obtained in the recorded chromatograms.

Kinetic and mineralization tests were duplicated and average values are reported. The error of the corresponding data within a 95% confidence interval was very small (< 2%) and hence, error bars are not shown in figures.

NH_4^+ was quantified by the standard indophenol blue method with an Alpkem Flow Solution IV flow injection system. The other cations were determined by inductively coupled plasma-optical emission spectroscopy. The concentration of NO_3^-, SO_4^{2-}, Cl^-, ClO_3^- and ClO_4^- was obtained by ion chromatography using a Kontron 465 LC fitted with a Waters IC-pack (150 mm × 4.6 mm)

anion column at 35 ºC, coupled to a Waters 432 conductivity detector. A volume of 200 µL was injected into the LC upon elution of a sodium tetraborate, sodium gluconate, boric acid, butanol, acetonitrile and glycerine solution at 2 mL min^{-1}. Active chlorine was measured by the *N*,*N*-diethyl-*p*-phenylenediamine colorimetric method (λ = 515 nm) on a Shimadzu 1800 UV/Vis spectrophotometer (APWA, AWWA, WEF, 2005).

Stable organic intermediates accumulated after 30 and 120 min of degradation of 0.561 mM tetracaine in simulated matrix by PEF with BDD/air-diffusion cell at j = 33.3 mA cm^{-2} were identified by GC-MS, comparing with NIST05 data library. The treated solutions were lyophilized and the remaining solid was dissolved with 2 mL of CH_2Cl_2. Analysis was carried out on an Agilent Technologies 6890N GC coupled to an Agilent Technologies 5975C inert XL MS in EI mode at 70 eV. A non-polar Teknokroma Sapiens- X5ms (0.25 µm, 30 m × 0.25 mm) column was employed. The temperature program was: 36 ºC for 1 min, 5 ºC min^{-1} up to 325 ºC and hold time 10 min, with the inlet, source and transfer line at temperatures of 250, 230 and 300 ºC, respectively.

3. Results and discussion

3.1. Tetracaine degradation in 0.050 M Na_2SO_4

The degradation profiles obtained for the treatment of 150 mL of 0.561 mM tetracaine hydrochloride solutions by the different EAOPs were firstly assessed in 0.050 M Na_2SO_4 to clarify the oxidation power of hydroxyl radicals and/or UVA light. The study was carried out with a BDD anode since it is expected to be the best one in this synthetic medium (Panizza and Cerisola, 2009; Sirés and Brillas, 2012). Experiments were made after adjustment of the initial pH to 3.0 and addition 0.50 mM Fe^{2+} in EF and PEF. A constant j = 33.3 mA cm^{-2} was applied for 360 min. In all cases, the solution pH underwent a slight decay along time up to final values of 2.6-2.7, suggesting the formation of acidic byproducts like short-chain aliphatic carboxylic acids (Moreira et al., 2013,

226 Steter et al., 2016), since no pH change was found under similar electrolytic conditions for a
227 solution without contaminant.

228 Fig. 1a illustrates the tetracaine concentration decay with electrolysis time for the above assays.
229 A continuous removal of the pharmaceutical following an exponential decay up to its total
230 disappearance at long time can be observed in EO-H_2O_2, as expected if it is slowly attacked by
231 BDD($^{\bullet}$OH) originated from reaction (2). In contrast, only 180 min were needed for its
232 disappearance in EF and PEF systems, as a result of faster destruction by additional $^{\bullet}$OH produced
233 from Fenton's reaction (6). For the latter two EAOPs, a very quick degradation of tetracaine was
234 found during the first 5 min of electrolysis, whereupon it underwent a much slower removal up its
235 total disappearance. Fig. 1a also shows a quite analogous degradation rate by both, EF and PEF
236 treatments, thus informing about a very little production of $^{\bullet}$OH from photolytic reaction (8). The
237 inset panel of Fig. 1a shows the analysis of the above concentration decays assuming that tetracaine
238 obeyed a pseudo-first-order kinetics. A good linear correlation was obtained in EO-H_2O_2 trials,
239 giving rise to an apparent rate constant k_1 = 0.0106 min^{-1}. In EF and PEF processes, however, an
240 excellent linear correlation was only found for times > 5 min, related to k_1 ~ 0.02 min^{-1}. This
241 behavior can be associated with the fast and large conversion of Fe(II) into Fe(III) (about 90%) by
242 Fenton's reaction (6) (Sirés et al., 2014), yielding Fe(III)-tetracaine complexes that are more slowly
243 attacked by BDD($^{\bullet}$OH) and $^{\bullet}$OH than the initial molecule, as proposed for similar treatments of
244 other *N*-derivatives (Guelfi et al., 2017). The k_1 value obtained for each process along with its
245 regression coefficient (R^2) is summarized in Table 1. The pseudo-first-order decay of the
246 pharmaceutical suggests its reaction with a constant, low concentration of BDD($^{\bullet}$OH) and/or $^{\bullet}$OH in
247 all cases.

248 The TOC abatement for the above experiments, shown in Fig. 1b, reveals an enhancement of
249 the mineralization process in the order EO-H_2O_2 < EF < PEF, as can also be deduced from the final
250 TOC removal achieved, listed in Table 1. Again, the superiority of EF over EO-H_2O_2 can be

associated to the additional formation of •OH in the bulk, which outperform the BDD(•OH) because of their generation in the whole volume. The highest oxidation power was found in PEF system, which can be ascribed to the rapid photolysis of several organic intermediates, especially complexes of Fe(III), under UVA irradiation (Sirés and Brillas, 2012; Sirés et al., 2014). Nonetheless, partial mineralization was attained due to the high stability of remaining byproducts (see Table 1).

At the end of the PEF process, it was found that the solution contained 0.378 mg L^{-1} NH_4^+ (26.2% of initial N) and 0.135 mg L^{-1} NO_3^- (2.7% of initial N) coming from the mineralization of the N atoms of tetracaine (1.122 mM). Since the solution TN practically did not undergo any significant variation, one can conclude that NH_4^+ is the preponderant ion released during PEF, although most of the initial N remained in solution, probably as linear byproducts that are hardly removed by BDD(•OH), •OH and UVA light. Note that Lacasa et al. (2014) showed the partial reduction of NO_3^- to NH_4^+ in sulfate medium by EO using cathodes like conductive diamond, stainless steel, silicon carbide, graphite or lead. Nevertheless, this reaction is expected to be insignificant in our air-diffusion cathode, which is highly electrocatalytic for the reduction of O_2 gas to H_2O_2 by reaction (1). From these findings, the theoretical mineralization reaction of the protonated form of tetracaine, the prevailing species at pH = 3.0, can be written as reaction (10), yielding CO_2 and NH_4^+ as major generated nitrogenated ion upon passage of a number of electrons n = 74:

$$C_{15}H_{25}N_2O_2^+ + 28H_2O \rightarrow 15CO_2 + 2NH_4^+ + 73H^+ + 74e^- \quad (10)$$

The mineralization current efficiency (MCE) for each trial at current I (= 0.100 A) and electrolysis time t (h) was then estimated as follows (Thiam et al., 2015a; Steter et al., 2016):

$$\%\,\mathrm{MCE} = \frac{n\,F\,V\,\triangle(\mathrm{TOC})}{4.32\times10^7\,m\,I\,t} \times 100 \quad (11)$$

where F is the Faraday constant (= 96,485 C mol^{-1}), V is the solution volume (= 0.150 L), $\triangle$(TOC) is the TOC abatement (mg L^{-1}), 4.32×10^7 is a conversion factor (= 3600 s h^{-1} × 12,000 mg C mol^{-1}) and m is the number of carbon atoms of tetracaine (= 15).

The current efficiencies calculated from Eq. (11) for the trials of Fig. 1b are presented in Fig. 1c. As expected, MCE rose as the oxidation power of the EAOP increased (see Table 1), reaching the highest value of about 35% after 120 min of PEF. It is noteworthy that current efficiency gradually decreased at long electrolysis time in all cases. This behavior is typical of EAOPs and can be explained by the progressive loss of organic load along with formation of more resistant byproducts (Panizza and Cerisola, 2009), thus making the processes more inefficient.

3.2. Tetracaine degradation in simulated matrix

In a second series of experiments, the treatment of 0.561 mM tetracaine hydrochloride in the simulated matrix at pH 3.0 was tested by the different EAOPs in order to know the influence of Cl^- ion on the degradation process. Initially, a BDD anode was used by applying the same conditions described for 0.050 M Na_2SO_4. The solution pH also underwent a slight drop with electrolysis time in all cases, attaining final values of 2.7-2.8 after 360 min of treatment at j = 33.3 mA cm^{-2}.

In all the above treatments, the accumulated H_2O_2 increased up to a steady state value, when its generation and destruction rates became equal, yielding 25.0, 14.5 and 6.1 mg L^{-1} in EO-H_2O_2, EF and PEF, respectively. This agrees with the quicker removal of H_2O_2 with Fe^{2+} from Fenton's reaction (6) in EF and, additionally, with the enhancement of Fe^{2+} regeneration from photolytic reaction (8) in PEF. Moreover, a higher steady H_2O_2 content of 31.5 mg L^{-1} was found operating under EO-H_2O_2 conditions without tetracaine, suggesting that this oxidant is able to oxidize some organics during the electrochemical decontamination. A similar electrolysis in the absence of pharmaceutical and Cl^- ion yielded a greater steady H_2O_2 concentration of 34.0 mg L^{-1} and thus, the lower H_2O_2 accumulation in the simulated matrix can be related to its reaction with active chlorine from reaction (12) (Sirés et al., 2014; Steter et al., 2016).

298 $HClO + H_2O_2 \rightarrow Cl^- + O_2(g) + H_2O + H^+$ (12)

299 Fig. 2a highlights the very rapid destruction of the pharmaceutical by all EAOPs, always
300 disappearing in about 40 min. The removal was slightly slower by EO-H_2O_2 compared to EF and
301 PEF, which led to quite analogous degradation rate. A more rapid disappearance of tetracaine was
302 obtained in the simulated matrix, as compared with Fig. 1a. This can be related to its preponderant
303 oxidation by active chlorine (Cl_2/HClO) generated from reactions (3) and (4). The slightly greater
304 rate found in EF and PEF systems can then be ascribed to the concomitant reaction with •OH
305 originated from Fenton's reaction (6). It is noticeable that for the two Fenton-based EAOPs, a
306 uniform pharmaceutical decay was obtained during all the electrolysis. The fact that the degradation
307 was not decelerated at times > 5 min, in contrast to behavior found in 0.050 M Na_2SO_4, suggests
308 that the aforementioned Fe(III) complexes are rapidly destroyed by active chlorine. The inset panel
309 of Fig. 2a shows the good linear fittings determined assuming a pseudo-first-order kinetics for all
310 the EAOPs, as a result of the attack of a constant amount of active chlorine and hydroxyl radicals.
311 The corresponding k_1 value given in Table 1 for EO-H_2O_2 in the simulated matrix was 5.6-fold
312 higher than that in 0.050 M Na_2SO_4, whereas it was 3.7-fold and 4.0-fold greater for EF and PEF,
313 respectively, corroborating the higher effectiveness of active chlorine compared to BDD(•OH) and
314 •OH to destroy tetracaine. These results also demonstrate that the influence of Cl^- ions contained in
315 the commercial tetracaine on processes performed in 0.050 M Na_2SO_4 can be disregarded.

316 Surprisingly, the TOC decay for the above treatments showed that mineralization was upgraded
317 in the sequence EF < EO-H_2O_2 < PEF, as depicted in Fig. 2b. This means that chlorinated and non-
318 chlorinated byproducts were more easily destroyed by BDD(•OH) and active chlorine in EO-H_2O_2
319 compared to EF, because they probably form more recalcitrant Fe(III) complexes in EF that are
320 more resist better the attack of •OH in the bulk, as well as BDD(•OH) and active chlorine. This
321 hypothesis on the detrimental action of active chlorine is supported by two experimental evidences.
322 On the one hand, the large enhancement of mineralization under PEF conditions (see Fig. 2b),

which can be explained by the photolysis of Fe(III) complexes upon UVA irradiation. On the other hand, the loss of mineralization effectiveness in the simulated matrix (22% and 13% for EF and PEF, respectively) with respect to 0.050 M Na_2SO_4 (see Table 1), which can be ascribed to the formation of hardly oxidizable complexes of Fe(III) with chlorinated byproducts. The mineralization profile is also reflected in the relative MCE values obtained, given in Fig. 2c and Table 1. The current efficiency fluctuated from 14% to 16% in EO-H_2O_2, from 12% to 15% in EF and from 19% to 22% in PEF. This behavior suggests a quite constant mineralization rate in all cases.

The influence of active anodes like Pt, IrO_2-based and RuO_2-based ones on tetracaine degradation was comparatively checked for the most powerful EAOP, i.e., PEF process. Fig. 3a shows a quick abatement of the pharmaceutical regardless of the anode, being slightly accelerated in the order: Pt < IrO_2-based < BDD < RuO_2-based, with total disappearance at 40-60 min due to its preponderant reaction with active chlorine formed from reactions (3) and (4). This tendency seems contradictory based on the greater active chlorine production expected for active anodes as compared to BDD (Thiam et al., 2015a; Steter et al., 2016). This anomalous behavior could then be explained by the remarkable destruction of active chlorine due to its reaction with H_2O_2 from reaction (12).

The inset panel of Fig. 3a illustrates the pseudo-first-order decay kinetics found in all trials. As can be seen in Table 1, the greatest k_1 = 0.097 min^{-1} was obtained with the RuO_2-based anode, then decreasing a 15.4%, 23.7% and 44.3% with BDD, IrO_2-based and Pt, respectively. This trend can then be associated with the gradually lower content of active chlorine in the aqueous matrix at the beginning of the PEF treatment.

A very different behavior was found when TOC removal was measured. Fig. 3b highlights the poor mineralization rate in PEF process using the three active anodes, only allowing near 34-36% TOC decay with 9.2-9.8% current efficiency after 360 min (see Table 1). In contrast, the use of

348 BDD led to a much greater final TOC drop of 70% with 19% current efficiency. This confirms the
349 key role of BDD(•OH) to oxidize the chlorinated intermediates formed, having much higher
350 oxidation ability than Pt(•OH), IrO_2(•OH) and RuO_2(•OH) (Panizza and Cerisola, 2009).
351 Consequently, one can infer that BDD is the best anode to destroy tetracaine and its metabolites in
352 the simulated matrix by PEF, since the treatment takes advantage of a large synergistic action
353 between BDD(•OH), •OH, active chlorine and UVA light to foster their mineralization.

354 *3.3. Tetracaine degradation in urban wastewater*

355 The study of the PEF treatment of tetracaine with different anodes was extended to an urban
356 wastewater matrix adjusted to pH = 3.0. As occurred in the other media, solution pH decayed up to
357 slightly smaller values of pH 2.6-2.7 after 360 min of electrolysis at j = 33.3 mA cm^{-2} in all cases.

358 The decay in pharmaceutical concentration with electrolysis time when treating 0.561 mM
359 tetracaine spiked into the real wastewater sample using BDD, Pt, IrO_2-based or RuO_2-based anodes
360 is depicted in Fig. 4a. A quite similar profile can be observed using the three former electrodes,
361 leading to overall pharmaceutical removal in 90 min, whereas a more rapid decay occurred for
362 RuO_2-based anode with tetracaine disappearance in 60 min. All these trials agreed with a pseudo-
363 first-order degradation kinetics, as shown in the inset panel of Fig. 4a. Comparison of Fig. 3a and 4a
364 allows concluding that the pharmaceutical disappeared more slowly in the urban wastewater than in
365 the simulated matrix in all cases, as also corroborated by the smaller k_1 values determined with each
366 anode in the former medium (see Table 1). The slower destruction of tetracaine in the urban
367 wastewater can be ascribed to the partial consumption of M(•OH), •OH and pre-eminently active
368 chlorine by NOM. This competition was not so important in PEF with the RuO_2-based anode,
369 probably because it led to a greater active chlorine accumulation. Conversely, it was comparatively
370 more significant with BDD, suggesting a dramatic scavenging influence of NOM on BDD(•OH)
371 availability for tetracaine degradation.

Fig. 4b confirms the large inefficiency of Pt, IrO_2-based and RuO_2 based anodes for reaching a high degree of mineralization. Worth noting, greater TOC removal was determined in these cases compared to trials performed in the simulated matrix, even though the urban wastewater containing tetracaine hydrochloride accounted for a larger TOC = 112.2 mg L^{-1} (see Fig. 3b and Table 1). Hence, the presence of NOM was beneficial for the overall mineralization process, except for PEF with BDD since the same amount (70 mg L^{-1} TOC) was destroyed in both media at the end of the electrolyses, as deduced from data of Table 1. As commented for the simulated matrix, the higher mineralization in urban wastewater was reached using BDD, then corroborating that it is the best anode for the PEF treatment of tetracaine.

The oxidation ability of the potent PEF process with BDD was tested for tetracaine contents between 0.028 and 1.122 mM spiked into the urban matrix. A gradual exponential drop of pharmautical concentration can be observed in Fig. 5 in all these runs, which always obeyed a pseudo-first-order kinetics, as presented in the inset panel. The time needed for total removal rose with the initial concentration, being close to 40, 60, 80, 90 and 240 min for 0.028, 0.140, 0.280, 0.561 and 1.122 mM tetracaine, respectively. According to this, the corresponding k_1 value progressively decreased (see Table 1), meaning that it did not correspond to a true pseudo-first-order rate constant. Nevertheless, greater content of the pharmaceutical was removed when its initial concentration increased. For instance, at 30 min of electrolysis, 6.8, 33.7, 71.8, 99.1 and 182.1 mg L^{-1} tetracaine were removed starting from 0.028, 0.140, 0.280, 0.561 and 1.122 mM, respectively. It can then be inferred that the presence of a higher organic load is beneficial since it favors the reaction of tetracaine and its oxidation products with BDD($^{\bullet}OH$), $^{\bullet}OH$ or active chlorine (Sirés et al., 2014; Martínez-Huitle et al., 2015) This gradually greater oxidation ability was verified for the mineralization process. Table 1 reveals a decay in percentage of TOC removal from 74% for 0.028 mM to 30% for 1.122 mM, corresponding to an increasing amount of TOC removed from

12.8 to 63.6 mg L^{-1}. This means that, as a very remarkable feature, the PEF treatment with BDD becomes more effective for highly charged urban wastewater.

Finally, to clarify whether PEF with BDD was able to destroy the NOM and the intermediates of tetracaine in the real wastewater matrix, a long electrolysis with 0.561 mM of the pharmaceutical was carried out. A 78% TOC abatement was found at 11 h, attaining 100% mineralization at 24 h. This confirms that this EAOP is powerful enough to mineralize all the organic matter contained in polluted solutions, although a long electrolysis time is needed owing to the very slow destruction of the largely recalcitrant final byproducts.

3.4. Total nitrogen, inorganic ions and active chlorine

The fate of N and Cl contained in the simulated matrix and the urban wastewater with 0.561 mM tetracaine hydrochloride was determined for PEF process with BDD. Table 2 summarizes the initial and final values found for TN, inorganic ions and active chlorine. In both media, TN was reduced to a much larger extent with active anodes, primordially with the RuO_2-based one (loss of 34-41% of initial N), compared to non-active BDD (loss of about 2% of initial N). This can be related to the generation of volatile byproducts such as N_2, N_xO_y and/or chloramines, which can be formed from reaction between the large quantities of active chlorine produced in active anodes and NH_4^+ (contained in the matrices and/or generated upon mineralization). This explanation is supported by the large destruction of the initial NH_4^+, as shown in Table 2, which followed a similar sequence to the relative loss of TN for the different anodes in each matrix. Table 2 also highlights the same trend for the accumulation of NO_3^- from tetracaine, which was more largely accumulated with BDD anode, in agreement with its great mineralization ability. Nevertheless, the sum of the concentration of NH_4^+ and NO_3^- ions was always smaller than the corresponding TN value, suggesting that the final treated solutions still contained large quantities of organic *N*-derivatives, especially for the three active anodes where > 57% of the initial TOC remained in the final solutions (see Fig. 3b and 4b).

Regarding the fate of chlorinated ions, it should be noted that a much higher removal of initial Cl^- occurred using BDD (see Table 2), regardless of the matrix considered. It has been reported that BDD can oxidize Cl^- to active chlorine, which is consecutively transformed into ClO_2^-, ClO_3^- and ClO_4^- ions by reactions (13)-(15) (Thiam et al., 2015a; Steter et al., 2016):

$$HClO + H_2O \rightarrow ClO_2^- + 3H^+ + 2e^- \quad (13)$$

$$ClO_2^- + H_2O \rightarrow ClO_3^- + 2H^+ + 2e^- \quad (14)$$

$$ClO_3^- + H_2O \rightarrow ClO_4^- + 2H^+ + 2e^- \quad (15)$$

However, the data of Table 2 also reveal an analogous final active chlorine concentration using all the anodes in each aqueous matrix, with slightly greater accumulation using the RuO_2-based anode, as expected from the faster tetracaine decay reported with this electrode in Fig. 3a and 4a. In the simulated matrix, a greater accumulation of ClO_4^- compared to ClO_3^- was found in all cases (see Table 2). The maximum total content of both ions with Pt (1.952 mM) was even superior to 1.597 mM determined with BDD, demonstrating that reactions (14) and (15) occurred to similar extent at all electrodes. A mass balance of all chlorinated species detected in the simulated matrix reveals a good agreement with the initial chloride content (11.91 mM) using Pt (11.77 mM, i.e., 98.8% of initial Cl^-), IrO_2-based (10.25 mM, i.e., 86.1%) and RuO_2-based (11.83 mM, i.e., 99.3%). In contrast, a large decay was observed with BDD (5.71 mM, i.e., 47.9%), which could be ascribed to its greater oxidation ability to generate not only more chloro-organics that remain in the solution, but also volatile inorganic species, probably ClO_2 from ClO_2^- oxidation (Gómez-Gonzalez et al., 2009), as well as chloramines.

3.5. Detection of intermediates and final linear short-chain carboxylic acids

GC-MS analysis of organics extracted upon treatment of 0.561 mM tetracaine hydrochloride in simulated matrix by PEF with BDD allowed identifying one benzenic compound (**2**), three

444 monochloro- (**3**-**5**), two dichloro- (**6** and **7**) and one trichloro- (**8**) benzenic derivatives, and one
445 dichloro aliphatic product (**9**), whose characteristics are summarized in Table S1 of Supplementary
446 Material. The aromatic derivative **2**, 4-hydroxybenzoic acid, comes from the partial loss of the side
447 groups of the benzenic ring of tetracaine (**1)** via deamination and hydroxylation. The partial
448 cleavage of the side groups upon chlorination, oxidation, deamination, denitration, demethylation,
449 dechlorination and/or hydroxylation yields chlorinated aromatics **3**-**8**. Further cleavage of the
450 benzene moiety by chlorination and oxidation explains the formation of the chlorinated aliphatic **9**,
451 i.e., dichloroacetic acid methyl ester. The detection of these intermediates confirms the production
452 of chlorinated byproducts using aqueous matrices with Cl^-, as pointed out above.

453 Ion-exclusion HPLC analysis of the above treated tetracaine solution revealed the generation of
454 two linear carboxylic acids, namely fumaric (**10**) and oxalic (**11**) acids. The former acid is expected
455 to appear from the breaking of the benzene moiety, whereas the second one arises from the
456 oxidation of **10** and other longer aliphatic acids, being a final product that is directly mineralized to
457 CO_2 (Moreira et al., 2013; Sirés et al., 2014). Fig. 6a and b illustrates the time-course of these acids
458 under the same conditions described in Fig. 3. As can be seen, both acids were produced with all
459 electrodes to a similar extent, showing maximum concentrations between 180 and 240 min of PEF
460 treatment. This suggests that they are pre-eminently originated by the combined action of $^{\bullet}OH$
461 formed from Fenton's reaction (8) and UVA light, since they form Fe(III)-fumarate and Fe(III)-
462 oxalate complexes to large extent that are easily photolyzed under light irradiation (Sirés et al.,
463 2014; Martínez-Huitle et al., 2015). In these assays, very small contents < 0.87 and < 23.1 μM of **10**
464 and **11**, respectively, were found in the final solutions, corresponding to a total TOC < 0.6 mg L^{-1},
465 which is an insignificant value compared to the large residual TOC remaining in them (e.g., 30 mg
466 L^{-1} using BDD, see Fig. 3b). These results allow inferring that tetracaine degradation involves the
467 predominant production of other byproducts with a high content of N, as stated above, resulting
468 even more recalcitrant than short-chain aliphatic carboxylic acids.

469 *3.6. Reaction sequence for tetracaine mineralization*

470 Based on the intermediates detected, a plausible reaction sequence for tetracaine mineralization
471 by PEF in Cl^--containing medium is proposed in Fig. 7. In this route, $^{\bullet}OH$ at the anode surface and
472 from Fenton's reaction (8) as well as active chlorine (Cl_2/HClO) are assumed as the main oxidizing
473 agents. Moreover, for sake of simplicity, only the formation of Fe(III)-oxalate complexes is stated.

474 The path is initiated with the cleavage of the side aliphatic groups of the benzene moiety of **1**
475 either by deamination or hydroxylation to yield **2**, or with parallel chlorination over C-2 leading to
476 the chloro-amine derivative **3** with a methoxy group. Further degradation of **3** yields **4**, **5** or **6** via
477 oxidation of the amine to a nitro group, demethylation of the methoxy group or chlorination over C-
478 5, respectively. Subsequent denitration with chlorination of **4** produces the trichloro-derivative **8**,
479 which can also be formed from deamination with chlorination of **6**. Hydroxylation of compounds **5**,
480 **6** and **8** with loss of carboxy or carbomethoxy group as well as deamination or denitration originates
481 the dichlorohydroquinone **7**. Oxidation of aromatic intermediates with breaking of benzene ring
482 yields linear aliphatic products like the dichloro-derivative **9** and the carboxylic acid **10**.
483 Degradation of these aliphatic compounds eventually leads to the final acid **11**, which can be
484 directly oxidized to CO_2 at the anode. Alternatively, its Fe(III) complexes can be largely photolyzed
485 by UVA light with Fe^{2+} regeneration according to reaction (9).

486 **4. Conclusions**

487 The PEF process with non-active BDD anode is the best EAOP for the removal of tetracaine
488 spiked into urban wastewater at pH 3.0. This method yielded greater mineralization compared to
489 active Pt, IrO_2-based and RuO_2-based anodes since it took advantage of synergy between M($^{\bullet}OH$),
490 $^{\bullet}OH$, active chlorine and UVA light to destroy the oxidation products of the pharmaceutical. Total
491 mineralization was feasible by PEF with BDD at long electrolysis time. Tetracaine always decayed
492 at similar rate obeying a pseudo-first-order kinetics regardless of the anode, being only slightly

493 faster with the RuO_2-based one because it originated larger amounts of active chlorine. However,
494 the chlorinated products were largely recalcitrant using a Pt, IrO_2-based or RuO_2-based anodes,
495 therefore requiring BDD for their destruction. The fast photolysis of Fe(III) complexes upon UVA
496 irradiation explains the superior oxidation ability of PEF. In Cl^--containing media, TN was lost to a
497 large extent for all active anodes due to formation of chloramines. ClO_3^- and ClO_4^- ions were
498 produced with all the electrodes, but initial Cl^- disappeared significantly from solution only with
499 BDD, possibly by oxidation to ClO_2. A reaction sequence for tetracaine mineralization by PEF in
500 the presence of chloride ion has been proposed.

501 **Acknowledgements**

502 The authors thank the financial support from project CTQ2016-78616-R (AEI/FEDER, EU).
503 The FPI grant awarded from MINECO (Spain) to C. Ridruejo is acknowledged as well.

504 **References**

505 Al-Otaibi, F., Ghazaly, E., Johnston, A., Perrett, D., 2014. Development of HPLC-UV method for
506 rapid and sensitive analysis of topically applied tetracaine: its comparison with a CZE
507 method. Biomed. Chromatogr. 28(6), 826-830.
508 Ammar, S., Abdelhedi, R., Flox, C., Arias, C., Brillas, E., 2006. Electrochemical degradation of the
509 dye indigo carmine at boron-doped diamond anode for wastewaters remediation. Environ.
510 Chem. Lett. 4(4), 229-233.
511 APWA, AWWA, WEF, 2005. Standard Methods for the Examination of Water and Wastewater, 21
512 st Ed. Method Number 4500-Cl Chlorine (residual)–G. DPD Colorimetric Method, American
513 Public Health Association, Washington D.C., pp. 4–67 and 4-68.
514 Assumpção, M.H.M.T., Moraes, A., De Souza, R.F.B., Reis, R.M., Rocha, R.M., Gaubeur, I.,
515 Calegaro, M.L., Hammer, P., Lanza, M.R.V., Santos, M.C., 2013. Degradation of dipyrone

via advanced oxidation processes using a cerium nanostructured electrocatalyst material. Appl. Catal. A: Gen. 462-463, 256-261.

Bedolla-Guzman, A., Sirés, I., Thiam, A., Peralta-Hernández, J.M., Gutiérrez-Granados, S., Brillas, E., 2016. Application of anodic oxidation, electro-Fenton and UVA photoelectro-Fenton to decolorize and mineralize acidic solutions of Reactive Yellow 160 azo dye. Electrochim. Acta 206, 307-316.

Boye, B., Michaud, P.A., Marselli, B., Dieng, M.M., Brillas, E., Comninellis, C., 2002. Anodic oxidation of 4-chlorophenoxyacetic acid on synthetic boron-doped diamond electrodes. New Diamond Frontier Carbon Technol. 12(2), 63-72.

Brillas, E., Sirés, I., Oturan, M.A., 2009. Electro-Fenton process and related electrochemical technologies based on Fenton's reaction chemistry. Chem. Rev. 109(12), 6570–6631.

Brinzila, C.I., Monterio, N., Pacheco, M.J., Ciríaco, L., Siminiceanu, I., Lopes, A., 2014. Degradation of tetracycline at a boron-doped diamond anode: Influence of initial pH, applied current intensity and electrolyte. Environ. Sci. Pollut. Res. 21(14), 8457-8465.

Cañizares, P., Lobato, J., Paz, R., Rodrigo, M.A., Saez, C., 2005. Electrochemical oxidation of phenolic compound wastes with BDD anodes. Water Res. 39(12), 2687-2703.

Coria, G., Sirés, I., Brillas, E., Nava, J.L., 2016. Influence of the anode material on the degradation of naproxen by Fenton-based electrochemical processes. Chem. Eng. J. 304, 817-825.

Cruz-González, K., Torres-López, O., García-León, A., Brillas, E., Hernández-Ramírez, A., Peralta-Hernández, J.M., 2012. Optimization of electro-Fenton/BDD process for decolorization of a model azo dye wastewater by means of response surface methodology. Desalination 286, 63-68.

Cruz-González, K., Torres-López, O., García-León, A., Guzmán-Mar, J.L., Reyes, L.H., Hernández-Ramírez, A., Peralta-Hernández, J.M., 2010. Determination of optimum operating

parameters for Acid Yellow 36 decolorization by electro-Fenton process using BDD cathode. Chem. Eng. J. 160(1), 199-206.

Dirany, A., Sirés, I., Oturan, N., Özcan, A., Oturan, M.A., 2012. Electrochemical treatment of the antibiotic sulfachloropyridazine: Kinetics, reaction pathways, and toxicity evolution. Environ. Sci. Technol. 46(9), 4074-4082.

dos Santos, E.V., Sáez, C., Martínez-Huitle, C.A., Cañizares, P., Rodrigo, M.A., 2015. The role of particle size on the conductive diamond electrochemical oxidation of soil-washing effluent polluted with atrazine. Electrochem. Commun. 55, 26-29.

El-Ghenymy, A., Garrido, J.A., Rodríguez, R.M., Cabot, P.L., Centellas, F., Arias, C., Brillas, E., 2013. Degradation of sulfanilamide in acidic medium by anodic oxidation with a boron-doped diamond anode. J. Electroanal. Chem. 689, 149-157.

El-Ghenymy, A., Rodríguez, R.M., Brillas, E., Oturan, N., Oturan, M.A., 2014. Electro-Fenton degradation of the antibiotic sulfanilamide with Pt/carbon-felt and BDD/carbon-felt cells. Kinetics, reaction intermediates, and toxicity assessment. Environ. Sci. Pollut. Res. 21(14) 8368-8378.

Escher, B.I., Baumgartner, R., Koller, M., Treyer, K., Lienert, J., McArdell, C.S., 2011. Environmental toxicology and risk assessment of pharmaceuticals from hospital wastewater. Water Res. 45(1), 75-92.

Feng, L., Van Hullebusch, E.D., Rodrigo, M.A., Esposito, G., Oturan, M.A., 2013. Removal of residual anti-inflammatory and analgesic pharmaceuticals from aqueous systems by electrochemical advanced oxidation processes. A review. Chem. Eng. J. 228, 944-964.

Flox, C., Cabot, P.L., Centellas, F., Garrido, J.A., Rodríguez, R.M., Arias, C., Brillas, E., 2006. Electrochemical combustion of herbicide mecoprop in aqueous medium using a flow reactor with a boron-doped diamond anode. Chemosphere 64(6), 892-902.

564 Golovko, O., Kumar, V., Fedorova, G., Randak, T., Grabic, R., 2014. Seasonal changes in
565 antibiotics, antidepressants/psychiatric drugs, antihistamines and lipid regulators in a
566 wastewater treatment plant. Chemosphere 111, 418-426.
567 Gómez-Gonzalez, A., Ibanez, J.G., Vasquez-Medrano, R., Zavala-Araiza, D., Paramo-Garcia, U.,
568 2009. Electrochemical paired convergent production of ClO_2 from $NaClO_2$ and $NaClO_3$. ECS
569 Trans. 20(1), 91-101.
570 Guelfi, D.R.V., Gozzi, F., Sirés, I., Brillas, E., Machulek Jr., A., de Oliveira,S.C., 2017.
571 Degradation of the insecticide propoxur by electrochemical advanced oxidation processes
572 using a boron-doped diamond/air-diffusion cell. Environ. Sci. Pollut. Res. 24(7), 6083-6095.
573 Khataee, A., Akbarpour, A., Vahi, B., 2014. Photoassisted electrochemical degradation of an azo
574 dye using Ti/RuO_2 anode and carbon nanotubes containing gas-diffusion cathode. J. Taiwan
575 Inst. Chem. Eng. 45(3), 930-936.
576 Lacasa, E., Llanos, J., Cañizares, P., Rodrigo, M.A., 2012. Effect of the cathode material on the
577 removal of nitrates by electrolysis in non-chloride media. J. Hazard. Mater. 213-214, 478-484.
578 Khataee, A., Khataee, A., Fathinia, M., Vahid, B., Joo, S.W., 2013. Kinetic modeling of
579 photoassisted-electrochemical process for degradation of an azo dye using boron-doped
580 diamond anode and cathode with carbon nanotubes. J. Ind. Eng. Chem. 19(6), 1890-1894.
581 Marselli, B., Garcia-Gomez, J., Michaud, P.A., Rodrigo, M.A., Comninellis, C., 2003.
582 Electrogeneration of hydroxyl radicals on boron-doped diamond electrodes. J. Electrochem.
583 Soc. 150(3), D79-D83.
584 Martínez-Huitle, C.A., Rodrigo, M.A., Sirés, I., Scialdone, O., 2015. Single and coupled
585 electrochemical processes and reactors for the abatement of organic water pollutants: A
586 critical review. Chem. Rev. 115(24), 13362-13407.

587 Moreira, F.C., Boaventura, R.A.R., Brillas, E., Vilar, V,J,P., 2017. Electrochemical advanced
588 oxidation processes: A review on their application to synthetic and urban wastewaters. Appl.
589 Catal. B: Environ. 202, 217-261.
590 Moreira, F.C., Garcia-Segura, S., Vilar, V.J.P., Boaventura, R.A.R., Brillas, E., 2013.
591 Decolorization and mineralization of Sunset Yellow FCF azo dye by anodic oxidation,
592 electro-Fenton, UVA photoelectro-Fenton and solar photoelectro-Fenton processes. Appl.
593 Catal. B: Environ. 142-143, 877-890.
594 Oturan, M.A., Aaron, J.J., 2014. Advanced oxidation processes in water/wastewater treatment:
595 principles and applications. A review. Crit. Rev. Environ. Sci. Technol. 44(23), 2577-2641.
596 Özcan, A., Şahin, Y., Koparal, A.S., Oturan, M.A., 2008. Propham mineralization in aqueous
597 medium by anodic oxidation using boron-doped diamond anode. Experimental parameters'
598 influence on degradation kinetics and mineralization efficiency. Water Res. 42(12), 2889-
599 2898.
600 Panizza, M., Cerisola, G., 2009. Direct and mediated anodic oxidation of organic pollutants. Chem.
601 Rev. 109(12), 6541-6569.
602 Ribeiro, J., Purgato, F.L.S., Kokoh, K.B., Léger, J.-M., De Andrade, A.R., 2008. Application of
603 Ti/RuO_2-Ta_2O_5 electrodes in the electrooxidation of ethanol and derivants: Reactivity versus
604 electrocatalytic efficiency. Electrochim. Acta 53(27), 7845-7851.
605 Rivera-Utrilla, J., Sánchez-Polo, M., Ferro-García, M.A., Prados-Joya, G., Ocampo-Pérez, R., 2013.
606 Pharmaceuticals as emerging contaminants and their removal from water. A review.
607 Chemosphere 93(7), 1268-1287.
608 Santos, V., Diogo, J., Pacheco, M.J.A., Ciríaco, L., Morão, A., Lopes, A., 2010. Electrochemical
609 degradation of sulfonated amines on Si/BDD electrodes. Chemosphere 79(6), 637-645.

610 Scialdone, O., Randazzo, R., Galia, A., Filardo, G., 2009. Electrochemical oxidation of organics at
611 metal oxide electrode: the incineration of oxalic acid at IrO_2-Ta_2O_5 (DSA-O_2) anode.
612 Electrochim. Acta 54(4), 1210-1217.
613 Shubha, J.P., Puttaswamy, 2014. Oxidation of tetracaine hydrochloride by chloramine-b in acid
614 medium: Kinetic modelling. Adv. Phys. Chem. Article ID 238984, 8 pages.
615 Sirés, I., Brillas, E., 2012. Remediation of water pollution caused by pharmaceutical residues based
616 on electrochemical separation and degradation technologies: A review. Environ. Int. 40, 212-
617 229.
618 Sirés, I., Brillas, E., Oturan, M.A., Rodrigo, M.A., Panizza, M., 2014. Electrochemical advanced
619 oxidation processes: today and tomorrow. A review. Environ. Sci. Pollut. Res. 21(14), 8336-
620 8367.
621 Steter, J.R., Brillas, E., Sirés, I., 2016. On the selection of the anode material for the
622 electrochemical removal of methylparaben from different aqueous media. Electrochim. Acta
623 222, 1464-1474.
624 Thiam, A. Brillas, E., Centellas, F., Cabot, P.L., Sirés, I., 2015a. Electrochemical reactivity of
625 Ponceau 4R (food additive E124) in different electrolytes and batch cells. Electrochim. Acta
626 173, 523-533.
627 Thiam, A., Sirés, I., Garrido, J.A., Rodríguez, R.M., Brillas, E., 2015b. Decolorization and
628 mineralization of Allura Red AC aqueous solutions by electrochemical advanced oxidation
629 processes. J. Hazard. Mater. 290, 34-42.
630 Thiam, A., Zhou, M., Brillas, E., Sirés, I., 2014. Two-step mineralization of Tartrazine solutions:
631 Study of parameters and by-products during the coupling of electrocoagulation with
632 electrochemical advanced oxidation processes. Appl. Catal. B: Environ. 150-151, 116-125.
633 Vasudevan, S., Oturan, M.A., 2014. Electrochemistry: as cause and cure in water pollution-an
634 overview. Environ. Chem. Lett. 12(1), 97-108.

635 Vatanpour, V., Daneshvar, N., Rasoulifard, M.H., 2009. Electro-Fenton degradation of synthetic
636 dye mixture: influence of intermediates. J. Environ. Eng. Manage. 19(5), 277-282.
637 Wang, A., Qu, J., Liu, H., Ru, J., 2008. Mineralization of an azo dye Acid Red 14 by photoelectro-
638 Fenton process using an activated carbon fiber cathode. Appl. Catal. B: Environ. 84(3-4),
639 393-399.
640 Welcher, F.J., 1975. Standard Methods of Chemical Analysis, sixth ed, vol. 2, R.E. Krieger
641 Publishing Co, Huntington, New York, Part B.
642 Yahya, M.S., Oturan, N., El Kacemi, K., El Karbane, M., Aravindakumar, C.T., Oturan, M.A.,
643 2014. Oxidative degradation study on antimicrobial agent ciprofloxacin by electro-Fenton
644 process: Kinetics and oxidation products. Chemosphere 117, 447-454.

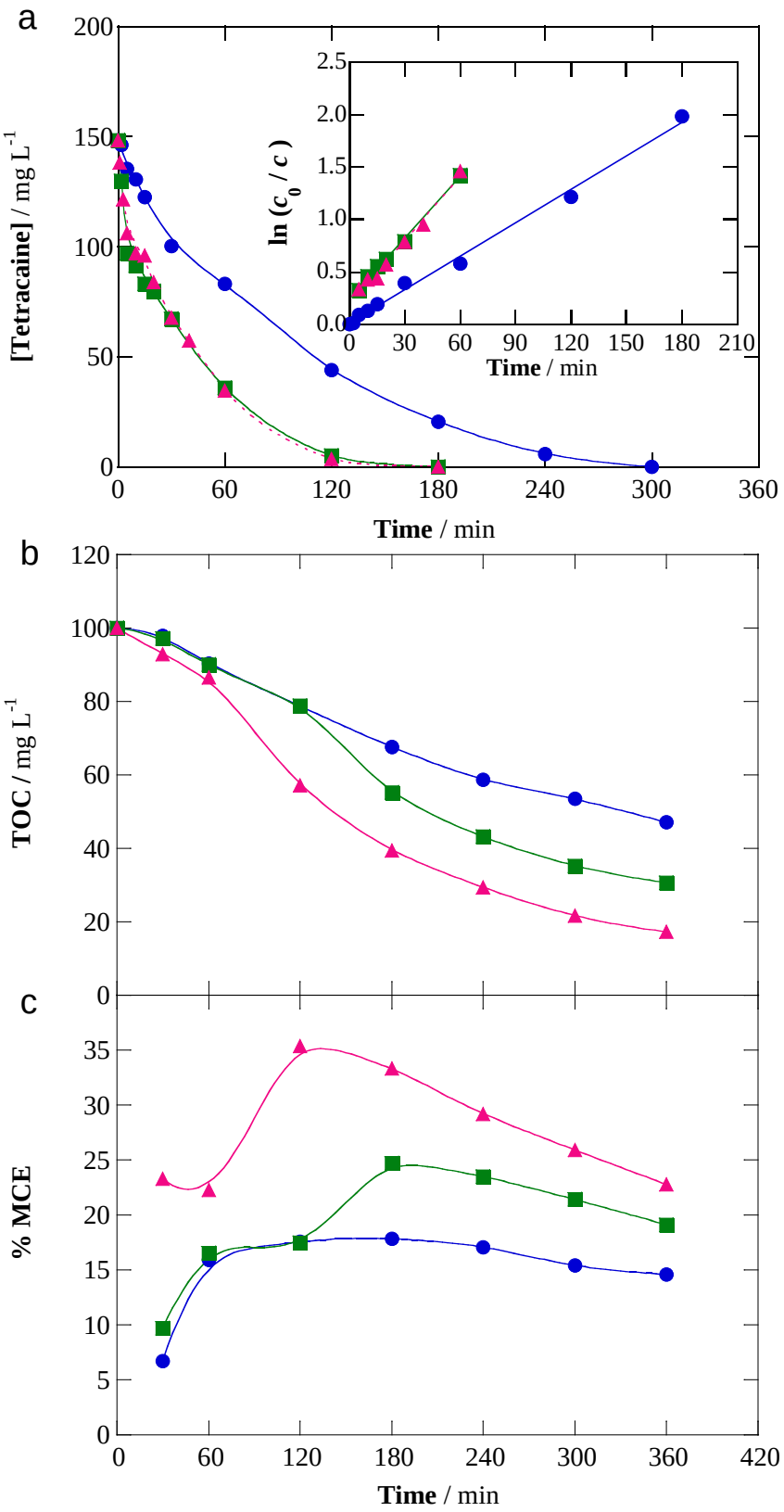

Fig. 1. (a) Tetracaine content decay, (b) TOC removal and (c) mineralization current efficiency with electrolysis time for the treatment of 150 mL of a 0.561 mM pharmaceutical solution in 0.050 M Na_2SO_4 at pH 3.0 using a boron-doped diamond (BDD)/air-diffusion cell, both electrodes with 3 cm^2 area, at current density (*j*) of 33.3 mA cm^{-2} and 35 ºC. Method: (●) Electrochemical oxidation with electrogenerated H_2O_2 (EO-H_2O_2), (■) electro-Fenton (EF) with 0.50 mM Fe^{2+} and (▲) photoelectro-Fenton (PEF) with 0.50 mM Fe^{2+} and 6 W UVA light. The inset panel of graph (a) presents the corresponding pseudo-first-order kinetic analysis.

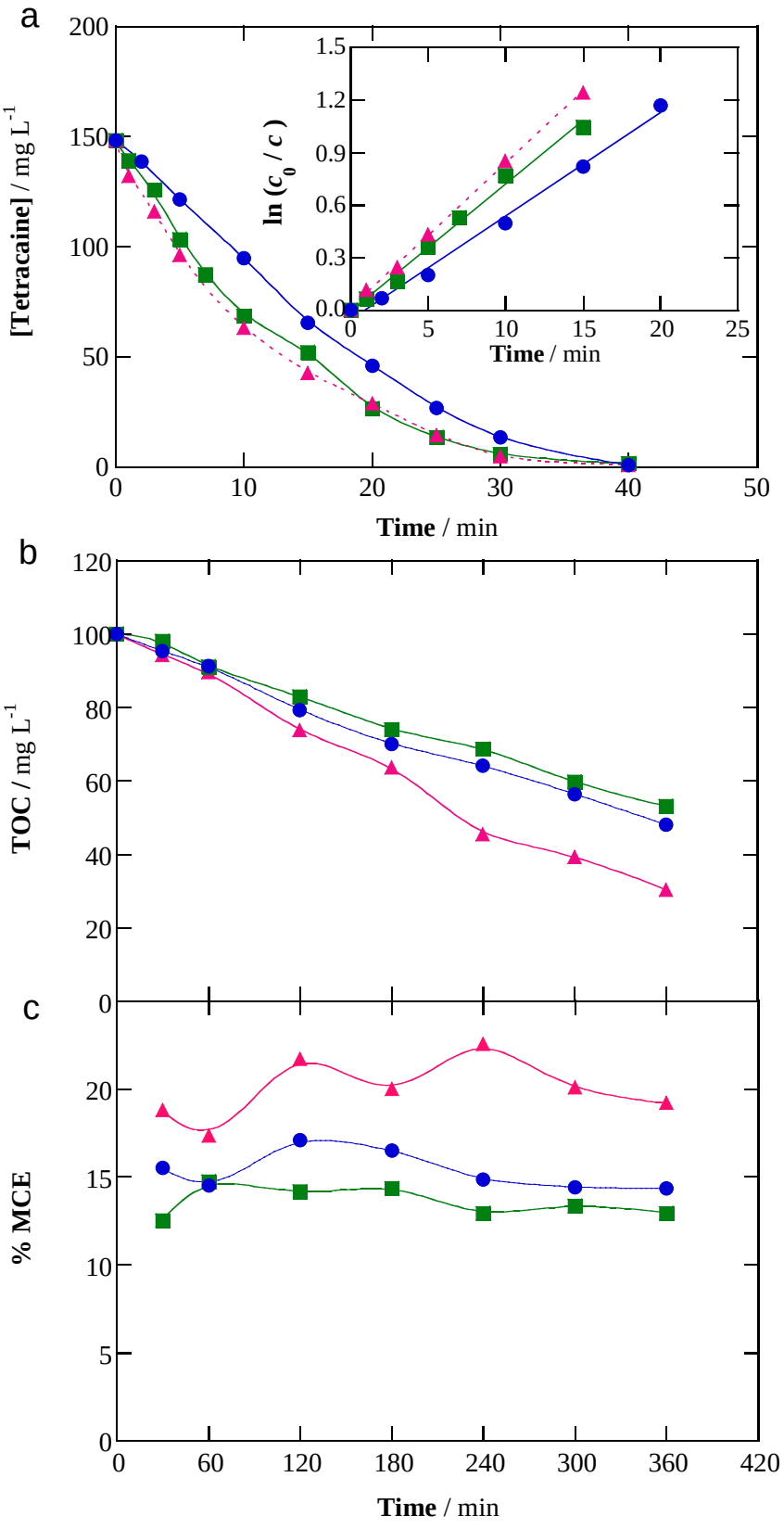

Fig. 2. (a) Tetracaine concentration removal, (b) TOC abatement and (c) mineralization current efficiency over time for the degradation of 150 mL of a 0.561 mM pharmaceutical solution in the simulated matrix at pH 3.0 using a BDD/air-diffusion cell at j = 33.3 mA cm^{-2} and 35 ºC. Method: (●) EO-H_2O_2, (■) EF with 0.50 mM Fe^{2+} and (▲) PEF with 0.50 mM Fe^{2+}. The inset panel of graph (a) depicts the kinetic analysis for a pseudo-first-order reaction of tetracaine.

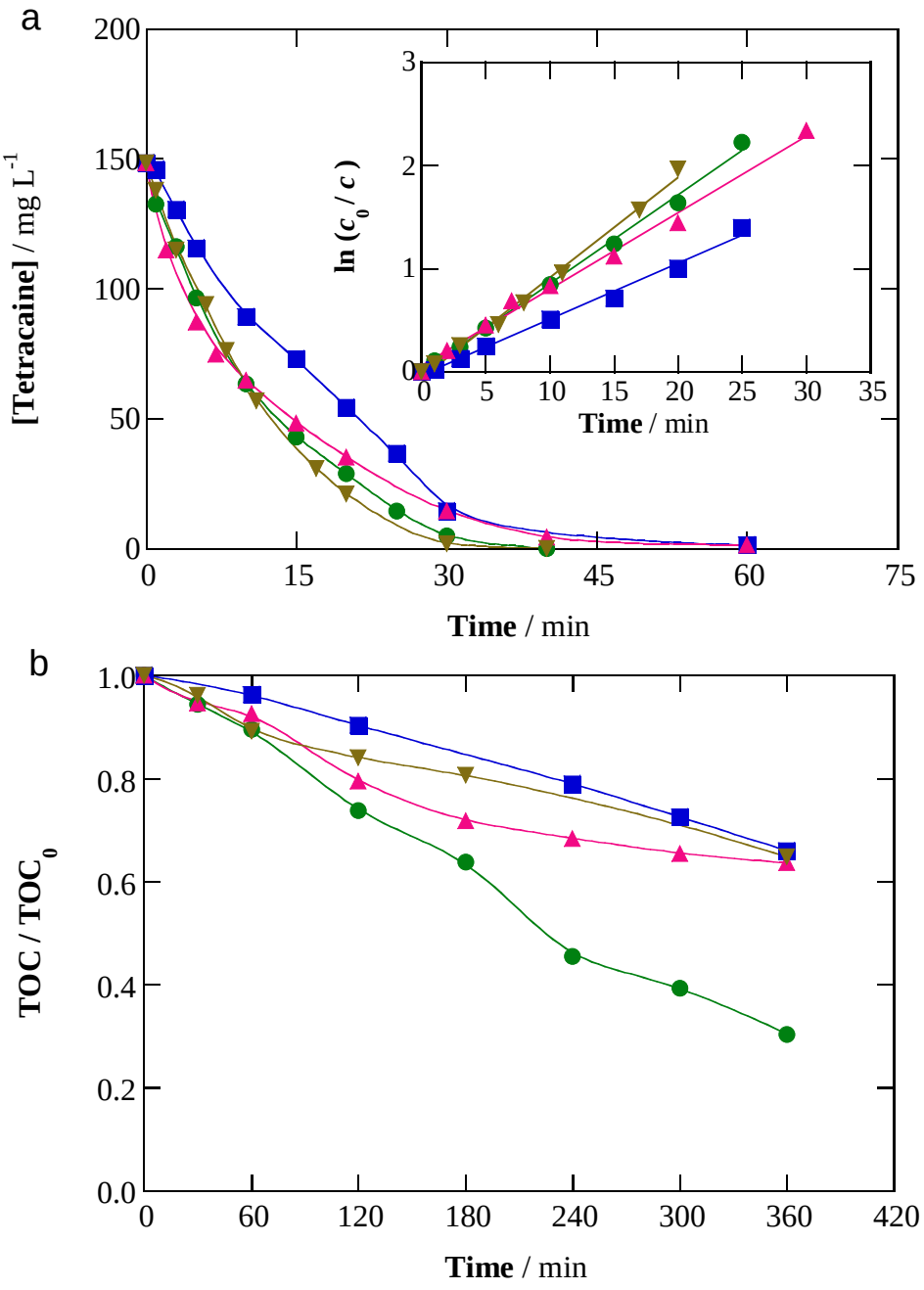

Fig. 3. (a) Drug concentration decay and (b) normalized TOC removal (initial TOC = 100 mg L^{-1}) for the PEF treatment of 150 mL of a 0.561 mM tetracaine solution in the simulated matrix at pH 3.0, j = 33.3 mA cm^{-2} and 35 ºC. Anode: (●) BDD, (■) Pt, (▲) IrO_2-based and (▼) RuO_2-based. The corresponding pseudo-first-order kinetic analysis is shown in the inset panel of Fig. 3a.

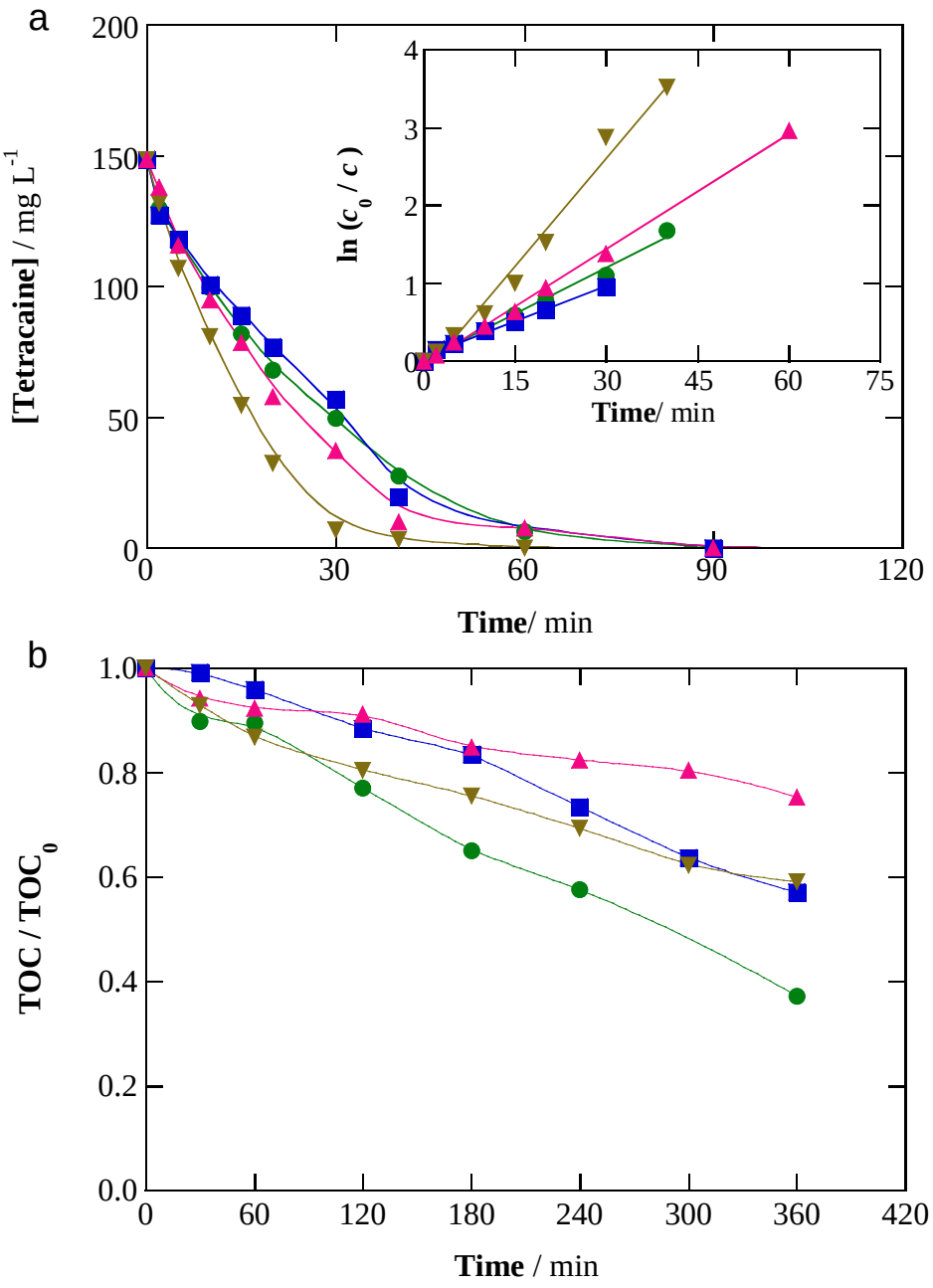

Fig. 4. (a) Drug concentration removal and (b) normalized TOC decrease (initial TOC = 112.2 mg L^{-1}) for the PEF treatment of 150 mL of 0.561 mM tetracaine spiked into urban wastewater at pH 3.0, j = 33.3 mA cm^{-2} and 35 ºC. Anode: (●) BDD, (■) Pt, (▲) IrO_2-based and (▼) RuO_2-based. The inset panel of Fig. 4a presents the kinetic analysis assuming a pseudo-first-order reaction for tetracaine.

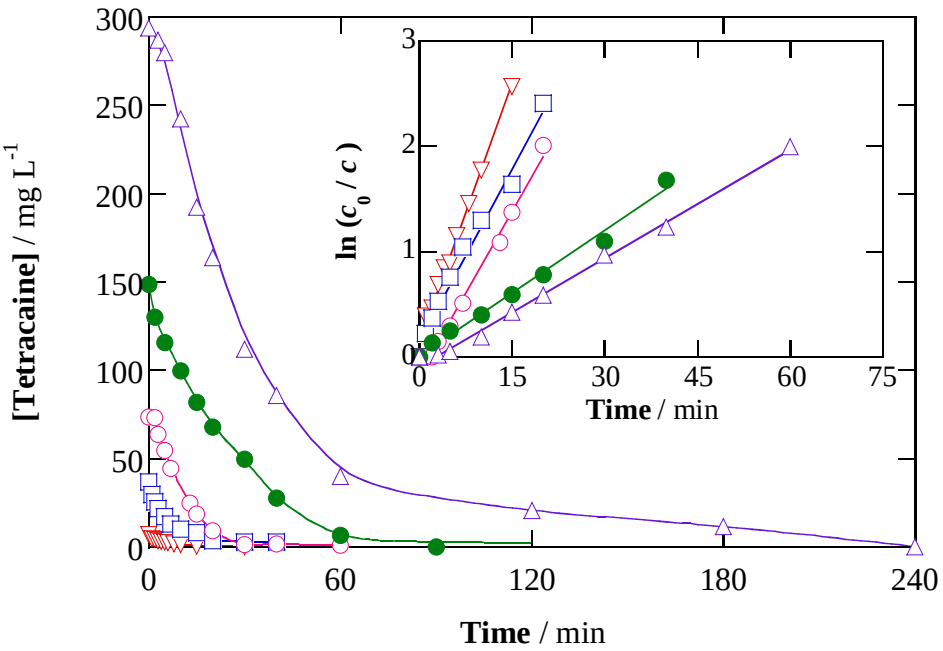

Fig. 5. Effect of tetracaine concentration on its decay kinetics for the PEF treatment of 150 mL of different solutions of the pharmaceutical spiked into urban wastewater at pH 3.0 using a BDD/air-diffusion cell at j = 33.3 mA cm^{-2} and 35 ºC. Initial tetracaine content: (△) 1.122 mM, (●) 0.561 mM, (○) 0.280 mM, (□) 0.140 mM and (▽) 0.028 mM. The inset panel presents the pseudo-first-order kinetic analysis.

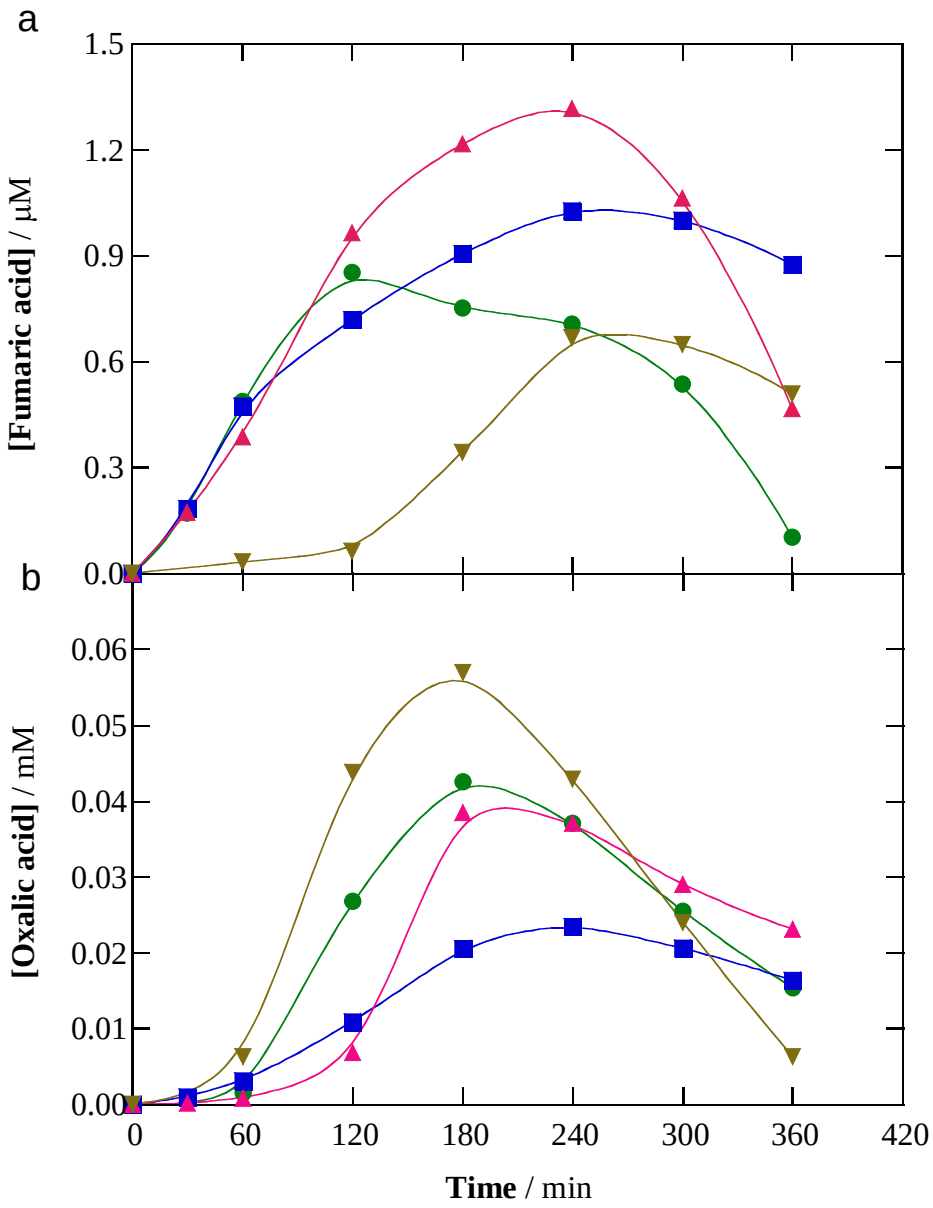

Fig. 6. Time-course of the concentration of (a) fumaric (**10**) and (b) oxalic (**11**) acids detected during the PEF treatment of a 0.561 mM tetracaine solution in the simulated matrix under the same conditions of Fig. 3. Anode: (●) BDD, (■) Pt, (▲) IrO_2-based and (▼) RuO_2-based.

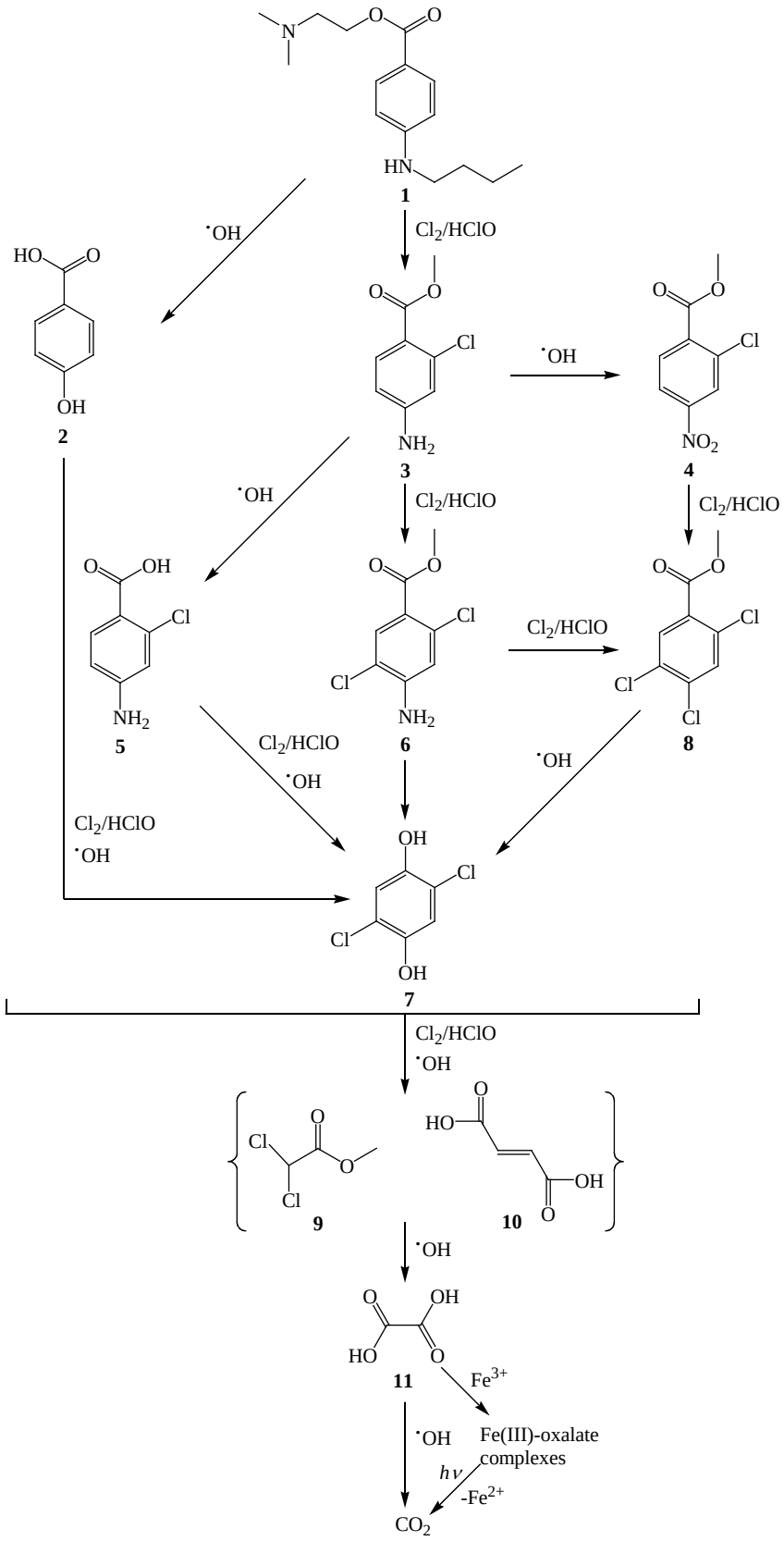

Fig. 7. Proposed reaction sequence for tetracaine mineralization by PEF in Cl^--containing medium. $^{\bullet}OH$ accounts for the hydroxyl radical formed at the anode surface and from Fenton's reaction. Cl_2/HClO denotes the active chlorine species originated from anodic oxidation of Cl^-.

Table 1.

Pseudo-first-order rate constant along with R-squared, percentage of TOC removal and mineralization current efficiency determined for the degradation of 150 mL of tetracaine in synthetic and urban wastewater at pH 3.0 by electrochemical advanced oxidation processes with different anodes and an air-diffusion cathode at j = 33.3 mA cm^{-2} and 35 ºC.

Method	Anode	$[Tetracaine]_0$ (mM)	k_1 (min^{-1})	R^2	% TOC removal	% MCE
0.050 M Na_2SO_4 solution						
EO-H_2O_2	BDD	0.561	0.0106	0.995	53[b]	15[b]
EF	BDD	0.561	0.0195[a]	0.997	69[b]	19[b]
PEF	BDD	0.561	0.0204[a]	0.987	83[b]	23[b]
Simulated matrix						
EO-H_2O_2	BDD	0.561	0.059	0.992	52[b]	14[b]
EF	BDD	0.561	0.073	0.998	47[b]	13[b]
PEF	BDD	0.561	0.082	0.992	70[b]	19[b]
	Pt	0.561	0.054	0.992	34[b]	9.3[b]
	IrO_2-based	0.561	0.074	0.992	36[b]	9.7[b]
	RuO_2-based	0.561	0.097	0.994	35[b]	9.5[b]
Urban wastewater						
PEF	BDD	0.028	0.163	0.992	74[c]	-
	BDD	0.140	0.109	0.984	49[c]	-
	BDD	0.280	0.103	0.986	37[c]	-
	BDD	0.561	0.040	0.990	23[c]	-
					35[d]	-
					63[b]	-
	Pt	0.561	0.030	0.991	43[b]	-
	IrO_2-based	0.561	0.049	0.998	25[b]	-
	RuO_2-based	0.561	0.092	0.990	41[b]	-
	BDD	1.112	0.034	0.995	30[d]	-

[a] From 5 to 60 min of treatment (Fig. 1a)

Electrolysis time: [b] 360 min, [c] 120 min, [d] 180 min

Table 2.

Total nitrogen and inorganic ions detected before electrolysis and after 360 min of PEF treatment of 150 mL of 0.561 mM tetracaine in simulated matrix and urban wastewater at pH 3.0 using different anodes and an air-diffusion cathode at j = 33.3 mA cm^{-2} and 35 ºC.

Parameter	Initial value	BDD (at 360 min)	Pt (at 360 min)	IrO_2-based (at 360 min)	RuO_2-based (at 360 min)
Simulated matrix					
TN (mM)	2.654	2.580	2.073	2.544	1.726
NO_3^- (mM)	0.0258	0.6523	0.3798	0.2770	0.1726
NH_4^+ (mM)	1.961	1.443	1.037	0.280	0.302
Cl^- (mM)	11.91	3.99	9.77	9.29	10.18
ClO_3^- (mM)	-	0.572	0.391	0.140	0.214
ClO_4^- (mM)	-	1.025	1.564	0.728	1.275
Active chlorine (mg L^{-1})	-	0.121	0.047	0.092	0.165
Urban wastewater					
TN (mM)	3.215	3.150	2.252	2.901	1.892
NO_3^- (mM)	0.0237	0.5291	0.4089	0.4347	0.4462
NH_4^+ (mM)	2.053	1.848	0.939	0.791	0.299
Cl^- (mM)	11.73	2.71	10.53	9.50	7.31
Active chlorine (mg L^{-1})	-	0.047	0.005	0.078	0.098